



Three-Way Spectral Decompositions of High-Performance Military Aircraft Noise

Tracianne B. Neilsen,* Aaron B. Vaughn,† Kent L. Gee,‡ and S. Hales Swift§

Brigham Young University, Provo, Utah 84602

Alan T. Wall¶

U.S. Air Force Research Laboratory, Wright–Patterson Air Force Base, Ohio 45433
and

J. Micah Downing** and Michael M. James**

Blue Ridge Research and Consulting, LLC, Asheville, North Carolina 28801

DOI: 10.2514/1.J057992

High-performance military aircraft noise contains large- and fine-scale turbulent mixing noise and broadband shock-associated noise. A three-way spectral decomposition quantifies the contribution from each noise type in the sound of a tied-down F-35B aircraft on a linear ground-based array spanning 35–152 deg. This large spatial aperture allows for detailed investigation into the spatial variation in broadband shock-associated noise and fine- and large-scale turbulent mixing noise. The spectral models used in the decomposition capture the main features of the measured spectra with three exceptions: 1) that the F-35B engine noise contains multiple spectral peaks in the maximum radiation region, 2) that the nonlinear propagation increases the high-frequency spectral levels, and 3) that the low-frequency levels in the maximum radiation region are less than those predicted by the large-scale similarity spectrum. The F-35B broadband shock-associated noise has the same characteristic shape and variation in peak frequency as overexpanded, laboratory-scale jets. However, the peak level and width exhibit different trends than laboratory-scale broadband shock-associated noise and those recently reported for the F/A-18E aircraft. The strengths and limitations of current models to represent the spatial variation in the spectral content of F-35B noise can guide research efforts to more fully understand the sound radiation.

Nomenclature

D	=	nozzle diameter, m
f	=	frequency, Hz
f_{peak}	=	peak frequency, Hz
L	=	shock-cell spacing, Hz
L_{BBSAN}	=	modeled broadband shock-associated noise spectral level, dB
L_{max}	=	maximum measured level for each engine thrust request, dB
L_{peak}	=	modeled peak level at each location, dB
M_c	=	convective Mach number
M_d	=	design Mach number of nozzle
M_j	=	average Mach number of fully expanded jet
R	=	radius in spherical coordinates, m
u_c	=	convective velocity, m/s
w_{sh}	=	width parameter
x	=	sideline distance, m
z	=	axial distance, m
β	=	jet off-design parameter

θ_c	=	polar angle from jet centerline, deg
θ	=	polar angle from engine inlet, deg
ϕ	=	azimuthal angle, deg

I. Introduction

NOISE-REDUCTION efforts for the latest generation of tactical aircraft are of increasing importance to both the military and civilian population. Noise-reduction designs can benefit from an increased understanding of the different noise components and their relative importance at different operating conditions. The noise generation mechanisms fall into two categories: turbulent mixing noise and broadband shock-associated noise. In the two-source theory for turbulent mixing noise [1–3], the maximum noise generation is caused by the large-scale turbulent structures' interaction with the ambient air; the partially correlated nature of these interactions yields distinct directivity. Fine-scale turbulent structures also interact with the ambient air to produce lower-level, omnidirectional noise. Because high-performance military aircraft engines do not produce an ideally expanded jet, broadband shock-associated noise (BBSAN) is also a significant component of the noise at small angles relative to the engine inlet. BBSAN results from the interaction of the large-scale turbulent structures and the quasi-periodic shock cells [4]. Screech tones, while important in laboratory-scale underexpanded jets [5], are less significant in overexpanded jets and not seen in the spectra from single-engine, high-performance military aircraft. The relative importance of the BBSAN and the large- and fine-scale turbulent mixing noise is explored across a wide spatial aperture near the F-35B via a three-way spectral decomposition. This decomposition is done at different engine powers and provides insights into where current models, developed for laboratory-scale jet noise, apply to high-performance military aircraft noise. This spectral decomposition helps identify where further investigation into noise source mechanisms is needed and lays the ground work for the development of a broadband equivalent source model for F-35B noise.

In the two-source theory of jet noise, different kinds of turbulent mixing noise come from fine- and large-scale turbulent structures [1,2]. An experimental study of supersonic jet noise reported by

Presented as Paper 2018-3146 at the 2018 AIAA/CEAS Aeroacoustics Conference, Atlanta, GA, 25–29 June 2018; received 8 October 2018; revision received 11 April 2019; accepted for publication 12 April 2019; published online 22 May 2019. Copyright © 2019 by the American Institute of Aeronautics and Astronautics, Inc. All rights reserved. All requests for copying and permission to reprint should be submitted to CCC at www.copyright.com; employ the eISSN 1533-385X to initiate your request. See also AIAA Rights and Permissions www.aiaa.org/randp.

*Associate Professor, Department of Physics and Astronomy, N283 ESC. Member AIAA.

†Undergraduate Student, Department of Physics and Astronomy, N283 ESC.

‡Professor, Department of Physics and Astronomy, N283 ESC. Senior Member AIAA.

§Postdoctoral Fellow, Department of Physics and Astronomy, N283 ESC. Member AIAA.

¶Research Physicist, Battlespace Acoustics Branch, 2610 Seventh Street, Building 441. Member AIAA.

**President and Senior Vice President, 29 N Market Street, Suite 700. Member AIAA.

Schlinder [6] and Laufer et al. [7] in the mid-1970s indicated that the sound radiated to the sideline of an ideally expanded jet and sound in the maximum amplitude region are distinctly different. The fine-scale turbulent structures distributed throughout the plume are relatively compact sources and radiate omnidirectionally. The large-scale turbulent structures have larger spatial coherence and thus produce high-amplitude, directional sound radiation. The noise radiated from the fine-scale structures is, therefore, most likely to be detected to the sideline of the jet. The relative contribution of these two noise sources depends on Mach number, jet temperature, and radiation angle [8,9].

Studies of these two types of mixing noise led to empirical similarity spectra, developed from far-field data from a range of cold and heated, ideally expanded, laboratory-scale jets by Tam et al. [10,11]. The large-scale similarity (LSS) spectrum, which has a relatively narrow peak and power-law decay on both sides, was reported to fit the jet noise for aft angles, in which the sound radiation is a maximum. On the other hand, the fine-scale similarity (FSS) spectrum, with its broader peak and a more gradual rolloff at both high and low frequencies, matched the spectra of noise radiated to the sideline and forward directions. In addition, Tam et al. proposed that the turbulent mixing noise at any radiation angle is a sum of LSS and FSS spectra. The agreement between the similarity spectra and laboratory-scale jets at a variety of operating conditions is summarized in Refs. [3,8–11]. A recent study of an ideally expanded, unheated, Mach 1.5 laboratory-scale jet showed that application of the similarity spectra in the geometric near field agreed with the far-field decompositions when care was taken in defining angles [12]. The effect of temperature on the noise spectra was explored by Liu et al. [13] using large-eddy simulations with good agreement, except in the maximum radiation region.

The similarity spectra also agree with many of the features of high-performance military aircraft noise. Schlinder et al. [14] first applied the LSS spectrum to noise in the maximum radiation direction from a high-performance military aircraft engine. Reference [15] contains the first comparison of both the FSS and LSS spectra to noise from a tied-down, high-performance military aircraft. The similarity spectra agree with the measured turbulent mixing noise with a few important exceptions, explained in Sec. II.A. Spectral comparisons have also been shown for a few elevated microphones 38.1 m from a tied-down F-35AA1: the first F-35 prototype [16,17] and recently for a few ground-based microphones near a tied-down F/A18-A/E [18]. In addition, Harker et al. [19,20] explain how the autocorrelation envelopes associated with the similarity spectra agree with the measured autocorrelation near the high-power, installed engine in Ref. [15]. Recently, Faranosov et al. [21] compared the similarity spectra to an azimuthal decomposition of an aircraft engine on a static test bench. All of these studies have focused solely on the turbulent mixing noise.

In addition to turbulent mixing noise, nonideally expanded jets produce BBSAN. Harper-Bourne and Fisher [4] first identified the primary features of BBSAN (distinctive spectral shape, peak frequency, and peak level) and provided a methodology for predicting these features based on constructive interference due to the relative phasing of the sources. A series of laboratory-scale experiments at the NASA Langley Research Center [22–24], confirmed the presence of and spatial variation in these three BBSAN features. Tanna [25] explored the relative importance of BBSAN to turbulent mixing noise. BBSAN becomes stronger as the jet Mach number M_j deviates more from the design Mach number M_d . BBSAN is evident in the forward quadrant (small inlet angles) where the turbulent mixing noise has lower levels. The prominence of BBSAN relative to turbulent mixing noise decreases when temperature increases because of the corresponding increase in turbulent mixing noise. After additional experimental results that explored the shock–turbulence interactions [23], evaluated the BBSAN spectral shape [26], and investigated the role of shock structures and jet mixing layer development [27], Tam et al. [28–30] proposed a more sophisticated BBSAN spectral model. More recently Kuo et al. [31] provided a simplification of Tam et al.'s model that works well for the first spectral peak of BBSAN.

The nature of BBSAN in high-performance military aircraft noise is now under investigation. Tam et al. [18] modeled the BBSAN at a few locations near a tied-down F/A-18E operating at afterburner and reported that BBSAN from a high-performance military aircraft agrees with only two of the four trends observed in nonideally expanded, laboratory-scale jets. They indicated that the distinctive BBSAN spectral shape is present and that the spectral peak frequency increases as the inlet angle increases, as seen in laboratory-scale jets, for seven locations. Four of these seven locations show opposite trends from laboratory-scale studies in the BBSAN peak level and width. Vaughn et al. [32] showed the first analysis of BBSAN characteristics as a function of engine condition for high-performance aircraft noise. Specifically, the BBSAN characteristics are compared when the F-35B operated at four engine conditions: 75% engine thrust request (ETR), 100% ETR (military power), 130% ETR (partial afterburner), and 150% ETR (maximum afterburner). The F-35B BBSAN peak frequency increases with increasing inlet angle at all four engine conditions, and the peak frequency rises with increasing ETR in agreement with prior laboratory-scale studies in which the temperature and Mach number were varied [31]. The variation in peak level and width of the F-35 BBSAN, however, do not agree with laboratory-scale studies nor the F/A-18E study. A direct comparison between the F/A-18E and F-35B BBSAN characteristics for the afterburning engine condition are presented in this Paper.

With the goal of increasing the understanding of the noise generation mechanisms from an F-35B engine operated at different ETRs, this Paper presents a comprehensive, three-way spectral decomposition of F-35B noise over a wide angular aperture. In addition to confirming the strengths and limitations of applying the large- and fine-scale similarity spectra to the F-35B noise, particular attention is given to examining if the dominant BBSAN peak in the F-35B spectra can be modeled using the prevailing theory. After an explanation of the spectral models (Sec. II), a brief description of the measurements is given (Sec. III). Examples of the three-way decomposition are provided (Sec. IV) from the 71-element ground array, which spanned 32 m and was located approximately 8–10 m from the estimated shear layer. The spectral decompositions are analyzed (in Sec. V) at both 75% ETR and 150% ETR (maximum afterburner). Spatial variation in level and peak frequency for all three components is presented in Appendix A.1. Broadband spatio-spectral error maps, in Sec. V.A, highlight regions in which the three spectral models do and do not adequately match the F-35B spectra. In Sec. V.B, the spatial variation in the BBSAN modeling parameters are compared to those reported for the F/A-18E. Appendix A also contains investigations into the applicability of the standard relationship between the BBSAN peak frequency and the convective speed and a preliminary look at using the Kuo et al. model [31] for the second BBSAN peak. These analyses provide insights into the relative significance of the different jet noise components for an F-35B operating at different ETR and how these agree and disagree with prior conclusions.

II. Background

Most previous spectral decompositions have either applied the Tam et al. [8,10] similarity spectra to support the two-source model of turbulent mixing noise or modeled the BBSAN components [28–31]. In Ref. [33], however, Viswanathan et al. proposed a spectral method for separating turbulent mixing noise and BBSAN, based on the work in Ref. [34]. Spectral scaling laws were applied to a large database of jet noise measurements. They found a consistent spectral shape could be obtained over a range of known jet velocities and temperatures. Master spectra were created for turbulent mixing noise from ideally expanded, subsonic jets using a least-square fit of the scaled spectra at different temperature ratios. The master spectra were scaled to fit ideally expanded, supersonic jet noise spectra at the same temperature using jet velocity and velocity scaling exponents. They noted that these master spectra did not match the high-frequency content of supersonic jet noise spectra because of nonlinearity. In Ref. [33] (Figs. 8, 9, 3, and 13), these master spectra were subtracted

from supersonic jet noise containing BBSAN to yield the shock component.

The Viswanathan et al. [33] scaling-law approach cannot be used to decompose the F-35B noise for several reasons. First, the jet temperature and velocity are not known by the authors. Second, the master spectra shown in Ref. [33] have a peak Strouhal number around 0.2, which is expected in the maximum radiation region but not at the forward angles where BBSAN is prominent. (An example of the spatial variation in the peak frequency for a high-performance military aircraft engine is provided in Ref. [35].) Third, the higher-frequency portions of the shock component contain not only the BBSAN but also, potentially, energy related to nonlinear propagation, as discussed by Viswanathan et al. in regard to Figs. 34 and 35 of Ref. [33]. Supporting evidence for this claim was presented by Petitjean et al. [5] in their detailed study of nonlinear propagation effects at small inlet angles for supersonic, imperfectly expanded, heat-simulated model jets.

Because of these considerations, the Tam et al. [10] empirical similarity spectra for turbulent mixing noise and Kuo et al.'s [31] BBSAN model are used to identify the contributions of the different noise sources. These two spectral models are described in this section.

A. Similarity Spectra for Turbulent Mixing Noise

Comparisons of the similarity spectra and spectra from high-performance military aircraft engines are limited. In the investigation by Schlinker et al. [14], the LSS spectral shape agrees reasonably well with the measured spectra at aft angles in the far field of a round-nozzle engine at its full-thrust set point, except for high frequencies at which the spectral slope was appreciably shallower than predicted by the LSS spectrum. Neilsen et al. [15] were the first to compare both the FSS and LSS spectra and their combination against the spectra from a tied-down high-performance military aircraft [36]. They evaluated the ability of one-third octave (OTO) band similarity spectra to match spectral levels on ground-based microphones located 11.7 m (approximately 18 nozzle diameters D) from the jet centerline that spanned a wide angular aperture. Even though the engine nozzle geometry was noncircular for this aircraft and one engine ran at idle power while the other engine cycled through different engine conditions, the similarity spectra agree with large portions of the measured spectra. Toward the sideline of the aircraft, the fine-scale similarity spectrum agreed well, while the large-scale similarity spectrum provided a reasonable fit to the general shape around the region of maximum radiation, with a few important exceptions. Combinations of the two similarity spectra were shown to match the data in between those regions. Surprisingly, at high engine powers, a combination of the two similarity spectra was also evident at the farthest aft microphones with inlet angle around 152 deg.

Three main features of high-performance military aircraft spectra are not accounted for by the similarity spectra. First, at high frequencies, the degree of congruity between the similarity and measured spectra changes with engine condition and angle. At high engine powers, the measured high-frequency slope is systematically shallower than the LSS spectrum [37], with the largest discrepancy occurring in the region of maximum radiation. The shallowness of the high-frequency slope, apparent even in the forward direction, is due to waveform steepening caused by nonlinear propagation [35,38–41]. This effect was sometimes ignored in previous laboratory-scale studies in which the fit in the peak frequencies was sacrificed to compensate for the steeper slope, whereas in this work, frequencies below 2000 Hz were primarily considered in fitting the similarity spectra in the maximum radiation region.

Second, the LSS spectrum does not account for the presence of multiple spectral peaks found in the maximum radiation regions. Seiner et al. [42] showed a dual lobe for very high-temperature laboratory-scale jets and attributed it to different types of Mach waves described by Oertel [43] with theoretical modeling provided by Tam and Hu [44]. More recently, Liu et al. [45] showed a similar separation of different types of propagating waves in numerical simulations of high-temperature, supersonic jets. For the OTO band

analysis of military aircraft engine noise in Ref. [15], two spectral peaks are evident, but subsequent narrowband studies of the F-35 have indicated there are more than two peaks in the spectra [46–48].

Third, the measured low-frequency spectral slope is steeper than predicted by the LSS spectrum in the maximum radiation region. However, farther aft, the low-frequency slope changes and agrees better with the similarity spectral decomposition. The steeper low-frequency slope in the maximum radiation region persists in the far field, as shown in Figs. 4 and 5 of Gee et al. [39]. No explanation for this phenomenon has been proposed.

These conclusions were further investigated in a preliminary comparison of one-third octave band similarity spectra to spectra from elevated microphones at a radial distance of 38.1 m from the first F-35 prototype AA1 [16,17]. While the resulting OTO band spectral decomposition appeared to agree with the previous aircraft noise decomposition [15], the decomposition in Ref. [17] was complicated by the presence of a ground interference dip near the peak frequency. Thus, confirmation of the similarity spectra's ability to match high-performance military aircraft noise is more straightforward for a ground-based array. In 2013, acoustical measurements were made near a tied-down F-35B [49] on a 71-element, ground-based array placed approximately 8 m from the estimated shear layer. Examples of how the similarity spectra agree with measurements along this ground array are shown in Sec. IV.

Differences between the similarity spectra and the measured high-performance military aircraft noise distribution could be related to the high temperature. To investigate the impact of temperature on spectral characteristics, Liu et al. [13,45] applied the similarity spectra to large-eddy simulations of jets with a range of temperatures, the highest one being similar to an afterburning military aircraft exhaust. They found good agreement with the similarity spectra with a few caveats. First, a dual peak in the spectra arises as temperature increases [45]. Second, the high-frequency mismatch in the maximum radiation region increases with temperature [13]. They also confirmed the presence of FSS noise at large inlet angles. These studies provide support for using the similarity spectra to study high-performance military aircraft noise.

B. BBSAN Models

In Ref. [4], Harper-Bourne and Fisher first proposed a methodology for predicting BBSAN. Each shock cell is treated as a source with relative phasing set by the convective velocity of the turbulent flow. They concluded that the level of BBSAN depends only on the nozzle pressure ratio. The BBSAN intensity was observed to go as β^4 , with $\beta^2 = M_j^2 - 1$ (for their convergent nozzle). For convergent-divergent nozzles, Ref. [28] indicates that the appropriate definition is $\beta^2 = M_j^2 - M_d^2$. The relationship between β^4 and the level of the BBSAN indicates a strong dependence on the strength of and resultant density fluctuations at the shocks.

Harper-Bourne and Fisher [4] also postulated that the peak frequency f_{peak} associated with the maximum BBSAN level is related to convective velocity u_c , convective Mach number M_c , and average shock-cell spacing L . At a specific observation angle θ_c , relative to the jet centerline, the radiation from all the shock-cell sources would interfere constructively at the frequency

$$f_{\text{peak}} = \frac{u_c}{L(1 - M_c \cos \theta_c)} \quad (1)$$

and harmonics of f_{peak} . The upper harmonics, however, were not observed in their measurements. The Harper-Bourne and Fisher model for BBSAN was tested with several laboratory-scale experiments. Tanna's [25] experiments confirmed that the BBSAN increases as β increases. Norum and Seiner's [23] experiments compared BBSAN measurements over a range of jet conditions and showed that the Helmholtz number associated with f_{peak} increases with β for overexpanded jets. Pao and Seiner [26] quantified the distinctive shape of the BBSAN peak that rises as f^4 below f_p and decays as f^{-2} above f_{peak} .

A later BBSAN model was developed from instability wave theory for the large-scale turbulent mixing noise by Tam et al. [28–30]. In this model, BBSAN is produced by the coherent scattering of the large turbulence structures as they pass through the quasi-periodic shock cells in the jet plume. Interaction between the large-scale turbulence structures and the quasi-periodic shock cells gives rise to time-dependent disturbances, which when radiated to the far field become BBSAN. In essence, the quasi-periodic shock cells form a waveguide for the large-scale turbulent structures. The quasi-periodic shock cells appear to first increase then decrease as β increases. Additionally, the intensity of BBSAN depends on the strength of the shock cells inside the plume, and shock-cell strength is determined by the difference between the nozzle design Mach number M_d and the fully expanded jet Mach number M_j . In Ref. [30], the model was extended from the original derivation for slightly imperfectly expanded jets to moderately imperfectly expanded jets.

In this waveguide model for BBSAN of moderately imperfectly expanded jets, the far-field BBSAN spectrum [Eq. (3.7) in Ref. [30]] depends on frequency f and location in spherical coordinates (R, θ_c, ϕ) and contains a summation over the different waveguide modes, with inharmonic modal frequencies. While this waveguide model allows for the prediction of multiple BBSAN peaks, it has some limitations. When the model is used to match measured BBSAN spectra, the required f_1 is usually greater than the first observed BBSAN peak frequency, making it tricky to apply the model. In addition, the modeled BBSAN spectrum exhibits more high-frequency partials than observed in measurements as well as deeper dips between subsequent harmonics [28].

In many cases, only the first peak of BBSAN is identifiable. This observation led Kuo et al. [31] to produce a simplified model for the primary BBSAN spectral peak. At (R, θ_c, ϕ), the contribution of the main BBSAN peak to the sound pressure level is

$$L_{\text{BBSAN}} = L_{\text{peak}} + 10 \log \left(\exp \left[- \left(\frac{f_{\text{peak}}}{f} - 1 \right)^2 / w_{\text{sh}}^2 \right] \right) \quad (2)$$

where the original Strouhal numbers have been replaced by frequencies, as the jet diameter and velocity are unknown for the F-35. L_{peak} is the peak spectral level in decibels that occurs at the peak frequency f_{peak} . The parameter w_{sh} relates to the width of the BBSAN peak and is typically chosen to match the spectral level at $f = 0.75 f_{\text{peak}}$. The advantages of this simplified model are that jet-related parameters are not necessary and the identification of L_{peak} and f_{peak} is straightforward. [As a point of clarification, Eq. (2) was referred to in a recent publication [18] as *Tam's model* but is referred to here as *Kuo et al.'s model*.]

III. Measurement

Noise from a tied-down F-35B (the short-takeoff vertical landing variant) was measured at Edwards Air Force Base in California, 6 September 2013. The Pratt & Whitney F135 engine was operated at a series of engine conditions from idle to 150% ETR. Measurements were conducted in the early morning hours, with temperature varying between 19.4 and 23.1°C, relative humidity between 37.6 to 45.7%, and an average wind speed of 3.3 kt. Noise from two variants of the F-35 was measured on semicircular arcs centered at the microphone array reference point (MARP), described by James et al. [49]. As most of the noise generated by supersonic jets is emitted from the turbulent mixing that occurs behind the jet, the MARP represents an estimated source location for many frequencies of interest and is used to define angles. As reported in Ref. [49], noise measurements of the F-35A (conventional takeoff and landing variant) were also made and exhibit the same spectral characteristic as the F-35B. Although the two variants' engines are substantially different, the similarity in the noise generated is likely because both are designed to take off from a tarmac. Nonlinear propagation effects from 19.1 to 305 m have been analyzed in Refs. [50,51]. In addition to the elevated mid- and far-field arrays discussed in Ref. [49], a ground-based array was deployed closer to the aircraft.

The noise measured on the 71-element, ground-based, linear array of microphones is analyzed in this Paper. This linear array was approximately 8 m (likely 7–9 nozzle diameters) from the estimated shear layer of an F-35B. The array spanned 32 m, corresponding to an angular aperture of 35–152 deg relative to the engine inlet and the MARP, as illustrated in Fig. 1. The 6.35 mm (1/4 in.) diameter microphones were spaced 0.45 m (18 in.) apart. Calibrated acoustic pressure waveform data were synchronously acquired with National Instruments PXI-4498 cards sampling at 204.8 kHz. Five or six measurements at each ETR yielded consistent spectra. The ground-based linear array provides the opportunity to analyze the spatial variation in the F-35B power spectral density (PSD) without interference from ground reflections. These data are used in several concurrent studies, including a correlation and coherence analysis [48] and as input to beam forming and acoustical holography [46,47] for source characterization.

IV. Results

The similarity spectra decompositions for F-35B jet noise from the ground-based linear array lend insight into the applicability of the current spectral models. Three guidelines are applied to match the similarity spectra to measured spectral shapes. First, the decompositions primarily strive for agreement in the peak-frequency region. Second, the contributions to the overall sound pressure level (OASPL) associated with the individual spectral components are constrained to grow or decay smoothly as a function of inlet angle. Third, the peak frequency of each spectrum is expected to vary smoothly as the inlet angle increases. Examples of similarity spectra fits are shown in Figs. 2–4 for select microphones when the engine was operated at 75% ETR.

The spectral decompositions at 75% ETR capture much of the spatial variation in the F-35B noise, with the same notable exceptions observed for a different high-performance military aircraft [15]. At the smallest inlet angles, the PSD contains BBSAN; a combination of Kuo et al.'s BBSAN model in Eq. (2) and the FSS spectrum matches the majority of the spectral shape, e.g., Fig. 2a. As the inlet angle increases, the relative strength of the BBSAN decreases, while the turbulent mixing noise associated with the fine-scale turbulent structures increases. As the inlet angle passes approximately 76 deg, the BBSAN is no longer evident, and the FSS spectrum matches the PSD, as in Fig. 2b. The FSS-only condition spans a very narrow angular range for 75% ETR; at approximately 80 deg, the LSS spectrum must be added in to reproduce the spectral shape, e.g., Fig. 3a. This combination region extends to approximately 105 deg, beyond which the addition of FSS spectrum no longer improves the agreement, and the LSS spectrum matches all except the high frequencies, e.g., Fig. 3b, which have elevated levels due to nonlinear propagation [50,51]. In the maximum radiation region (inlet angles approximately 110–140 deg at 75% ETR), the LSS spectrum captures the overall shape of the peak region of the PSD, e.g., Fig. 4a, but misses several important features: 1) multiple spectral peaks [46–48], 2) a shallower high-frequency slope (of f^{-2}) resulting from nonlinear propagation [38–41,50–52], and 3) a steeper low-frequency slope. All three features were noted in prior spectral decompositions of high-performance military aircraft [15,16,35],

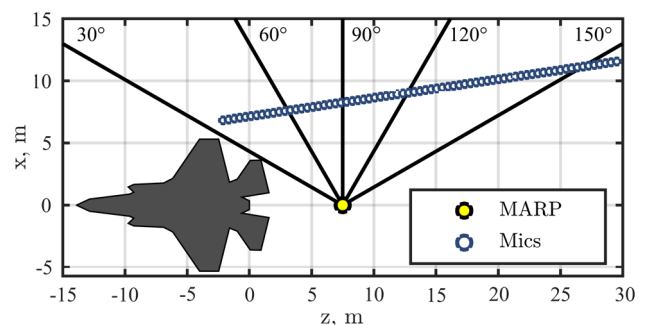


Fig. 1 Measurement geometry showing ground-based, 71 microphone array near an F-35 with inlet angles measured relative to the MARP.

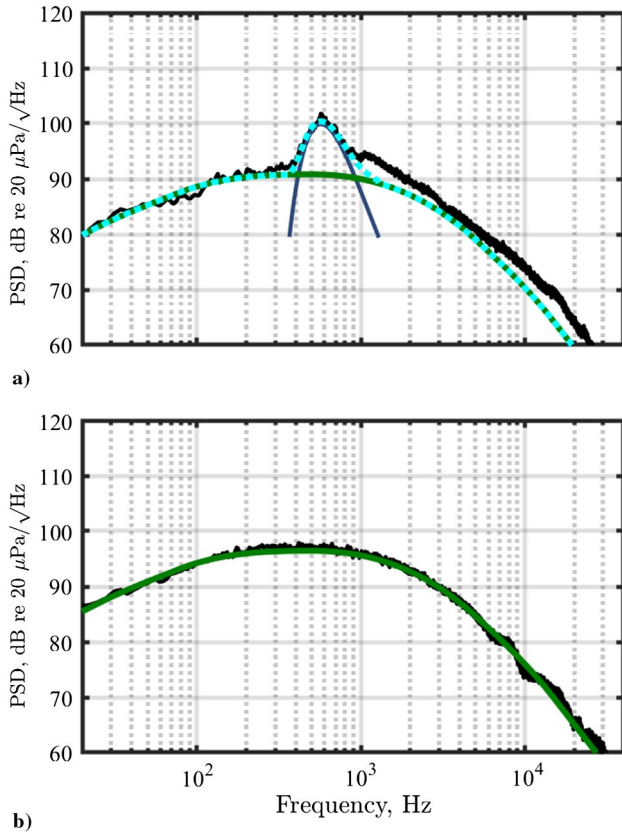


Fig. 2 PSD for 75% ETR (black) at a) 35 deg and b) 76 deg with FSS spectrum (green), Kuo et al.'s BBSAN model (blue), and total modeled PSD (cyan).

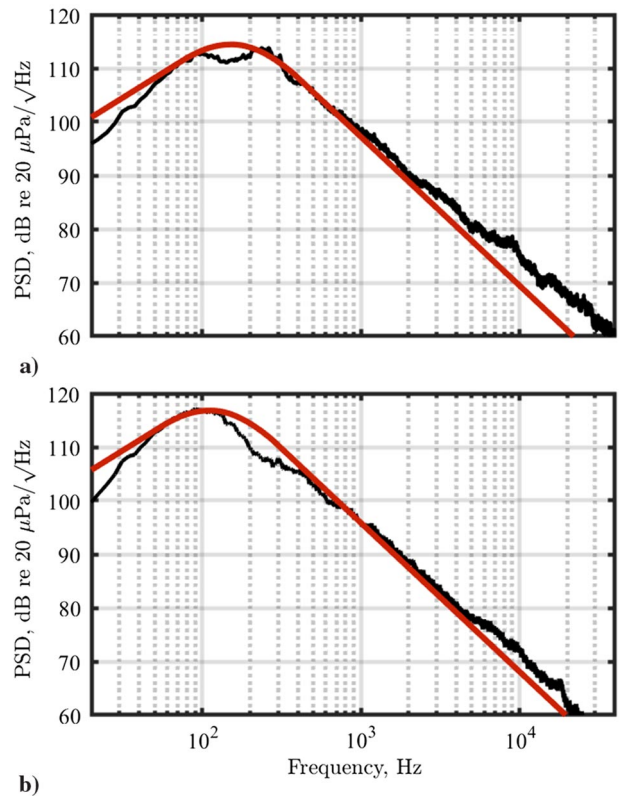


Fig. 4 PSD for 75% ETR (black) at a) 133 deg and b) 146 deg compared to the LSS (red) spectrum.

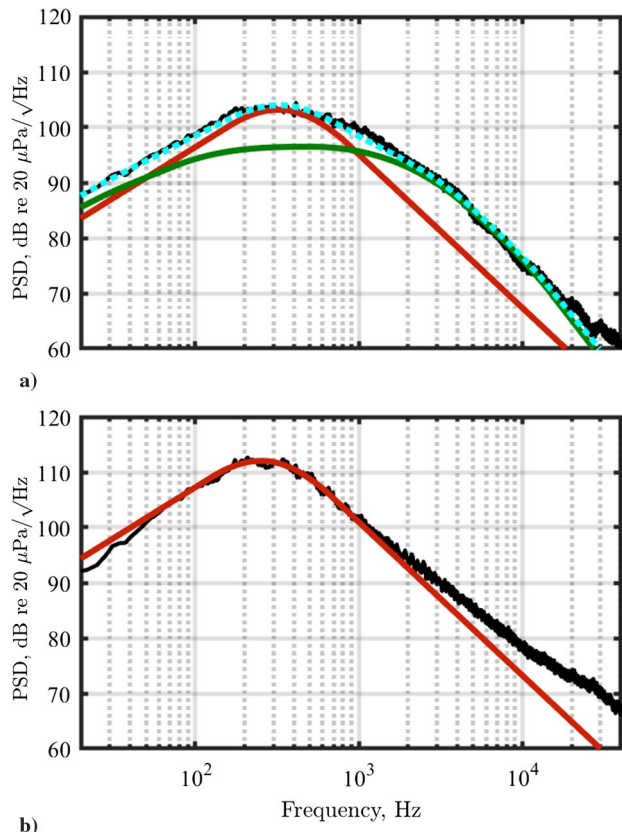


Fig. 3 PSD for 75% ETR (black) at a) 92 deg and b) 114 deg with FSS (green), LSS (red) spectra, and total modeled PSD (cyan).

and are discussed in more detail in Sec. V.A. Beyond the maximum radiation lobe, the PSD high-frequency slope steepens and better matches the LSS spectrum, e.g., Fig. 4b.

Although not obvious on the ground array at 75% ETR, for higher ETR, where the directivity has shifted farther, the high-frequency spectral shape shifts again at the largest angles, aft of the maximum radiation region. A better match to the PSD can be achieved when a combination of the LSS and FSS spectra is used, as displayed in Fig. 5 for 150% ETR at an inlet angle of 152 deg. This combination was first shown for different high-performance aircraft engine OTO band spectra in Fig. 8 of Ref. [15] and then at a closer location in Fig. 8 of Ref. [35]. It is hypothesized that the fine-scale turbulent structures radiate omnidirectionally and are apparent in the spectral shape aft of the maximum radiation lobe, when both the level and, perhaps more importantly, the peak frequency of the large-scale turbulent structures are lower. Analyses of spatial trends of the three-way spectral decomposition give insights into how the models for turbulent mixing noise and BBSAN spectra do and do not agree with spectral levels from the F-35B at different ETRs.

Questions naturally arise about the use of spectral models developed from far-field studies of laboratory-scale jets in evaluating the noise distribution closer to a full-scale aircraft. Several pieces of evidence imply that this process is worthwhile. First, a comparison was completed by Vaughn et al. [12] of near- and far-field spectral decompositions for an unheated, Mach 1.8, laboratory-scale jet, which showed that the similarity spectra agree with the spectra at 10 nozzle diameters, outside of the hydrodynamic near field, and that the same angular regions were represented by the FSS and LSS spectra when the angles were defined relative to a point 10 nozzle diameters from the nozzle exit. A longer discussion of near vs far field is provided in Appendix A.1. Second, Liu et al. [13] recently showed that the similarity spectra agree with far-field spectra computed with a large-eddy simulation for a jet temperature comparable to afterburning conditions with the exception of a dual spectral peak in the maximum radiation region. They even found that a match of LSS and FSS spectra represent the simulated spectra at 150 deg, similar to Fig. 5. Third, the similarity spectra have been compared to

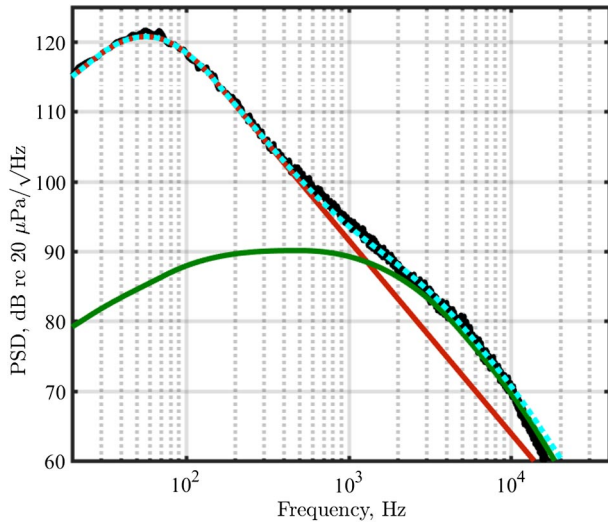


Fig. 5 PSD for 150% ETR (black) at 152 deg compared to the LSS (red) spectrum, the FSS (green), and the total modeled PSD (cyan).

the F-35B spectra from the elevated microphones along a 76 m arc (approximately 100 nozzle diameters). Except for the dips caused by the ground interference, the similarity spectra agree well with the measured far field with the same exceptions as those on the closer ground array: shallower high-frequency slope and dual peak in the maximum radiation direction. These studies support the applicability of the similarity spectra in analyzing the sound near high-performance military aircraft.

V. Analyses

The three-way spectral decomposition has provided a consistent framework for comparing BBSAN and turbulent mixing noise. An analysis of the peak levels and frequencies of each component for 75 and 150% ETR is provided in Appendix A.2. A comparison between the spectra modeled by the three-way decomposition and the measured PSD is shown as broadband error maps, in Sec. V.A, for the large angular aperture covered by the ground array. In Sec. V.B, The afterburning F-35B's BBSAN characteristics are compared to those reported by Tam et al. [18] for an afterburning F/A-18E. Estimates of the convective speed and shock-cell length when Eq. (1) is applied to the F-35 BBSAN peak frequencies are discussed in Appendix A.3. Finally, a preliminary application of the Kuo et al. BBSAN spectral model [31] for a second harmonic is given in Appendix A.4.

A. Errors

A concise way to view the overall performance of the three-way decomposition is with spatio-spectral error maps. These maps, shown in Fig. 6 for 75 and 150% ETR, contain differences between the F-35B PSD measured on the ground-based array and those predicted by the combined LSS, FSS, and BBSAN spectral models; these maps highlight combinations of frequency and location where the spectral decompositions do and do not agree well with the measurements. Many regions have remarkable agreement with less than ± 2 dB differences between the measured and modeled PSD. This agreement indicates that the combination of the turbulent mixing noise similarity spectra and Kuo et al.'s BBSAN model account for large portions of the radiated sound. The regions with larger differences correspond to limitations of using these spectral models for high-performance military aircraft noise.

The largest positive differences occur at high frequencies in the maximum radiation direction, where the measured spectral levels are higher than LSS spectrum. The sound levels received in this region (roughly 100–145 deg) are sufficiently large for cumulative nonlinear propagation to steepen the pressure waves and thus change the high-frequency spectral slope from the -28 dB/decade predicted by the LSS spectrum toward the -20 dB/decade slope associated with nonlinear propagation [38–41,52]. This change is greatest at the

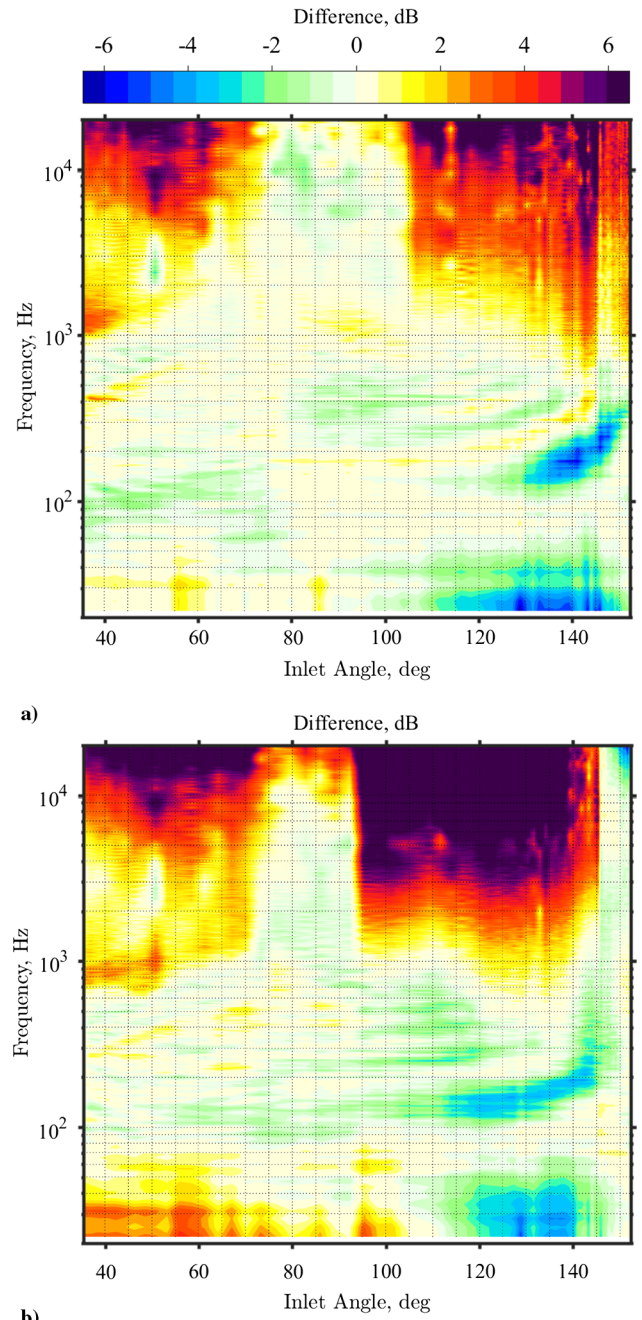


Fig. 6 Differences between measured PSD and the PSD of the three-way spectral decomposition (FSS + LSS + BBSAN) at a) 75% ETR and b) 150% ETR.

highest frequencies and affects progressively lower frequencies over a wider angular aperture as ETR increases. Evidence for cumulative nonlinear propagation effects for the tied-down F-35 is presented in Refs. [50,51]. The differing high-frequency slope confirms what was reported for a different aircraft engine's noise in Ref. [35].

In the forward direction (low values of θ), the high-frequency measured spectral levels are also larger than the modeled values. Higher-frequency BBSAN components cause the extra energy seen around 1000 Hz for $\theta < 50$ deg. A preliminary attempt to model higher-frequency components of the BBSAN is presented in Appendix A.4. At frequencies around 10 kHz and higher, the extra energy in the measured spectra could also be due to waveform steepening. A high-frequency spectral slope of $1/f^2$ (as expected for shock-containing waveforms) at small inlet angles was first established in Ref. [33] and was shown for a heat-simulated, supersonic, laboratory-scale jet at $\theta = 35$ deg in Ref. [5] and for a different tactical military aircraft engine in Fig. 6 of Ref. [35]. At

150% ETR for the F-35B measurements used in this Paper, the skewness of the time derivative of the pressure waveforms at forward locations have values larger than 5 in Fig. 5 of Ref. [51], a significant value as analytical work has shown that a threshold of 5 indicates the presence of acoustic shocks [53].

Two possible explanations arise as to why this shallower high-frequency slope is not observed in the middle angular region (roughly centered around 85 deg). First, it is possible that the combination of the LSS and FSS spectra used in this angular range provides enough flexibility to fit the spectral changes due to waveform steepening. This possibility is constrained, however, by the fairly strict requirements of smoothly varying OASPL and constant peak frequency for the FSS spectrum that guide the fitting process. Second, the low field coherence in this mixing region likely reduces the rate at which the waveform steepening occurs. This possibility is supported by studies of field coherence for the linear ground array near the F-35B in Ref. [48] and for a different military aircraft engine in Ref. [20]. The low coherence explanation for the lack of waveform steepening would also perhaps explain why the spectra at the smallest inlet angles again have a shallower high-frequency slope: the strong BBSAN component of the noise in that region is likely highly correlated.

At the largest inlet angles, the high-frequency portion of the spatio-spectral maps also shows fewer differences. For the 75% ETR case, the error decreases for $\theta > 145$ deg relative to the LSS spectrum. This decrease in spectral error agrees with the decreases in nonlinear propagation effects in this region quantified with different nonlinearity metrics by Reichman et al. [51]. A similar decrease in error is seen around 140–145 deg at 150% ETR. For larger θ , however, a distinctive shift occurs in the high-frequency spectral slope, a kink, at which point the FSS spectrum is again added to the spectral model. This downstream combination region occurs aft of a location when the LSS spectrum matches large portions of the high-frequency slope [15,35]. For the higher engine powers, the maximum radiation region for the large-scale turbulent mixing noise has shifted farther from the jet axis (Fig. A1b) and has a significantly lower peak frequency (Fig. A2b), such that the fine-scale mixing noise can be detected in the spectral shape. The addition of the FSS spectrum aft of the maximum radiation region at high engine powers follows the work in Ref. [15]; the combination of the LSS and FSS spectra, with the same peak frequency for the FSS spectrum as at smaller θ , improves the high-frequency fit, as in Fig. 5.

Looking now at the middle-frequency range on Fig. 6, the negative differences in the 100–800 Hz range between 110 and 145 deg come from dips in the measured PSD between the multiple frequency peaks. (See Fig. 4a for an example.) In the spatio-spectral error maps in Fig. 6, these dips are seen as striations and correspond to multiple spectral peaks occurring at different angles in the maximum radiation region. These multiple spectral peaks are a manifestation of the multiple spatial lobes that have been observed in the sound field around high-performance military aircraft. Evidence for and characterization of these multiple lobes for the F-35 are given in Refs. [46–48] and for a different aircraft engine in Refs. [15,20,35,54].

The large positive differences below 100 Hz in the maximum radiation region are a curious feature. These differences correspond to the fact that the LSS spectral slope below the peak frequency is shallower than is observed in the measurements. Examples are shown for 75% ETR in Fig. 6. This low-frequency discrepancy was also observed in Refs. [15,16] for different aircraft engines but not in laboratory-scale jet spectral decompositions in Ref. [12], which were performed using the same methods as in this Paper. The reason for the steep low-frequency slope in the maximum radiation region at both 75 and 150% ETR is unknown at the present time, but it appears to persist into the far field, as shown in Figs. 4 and 5 of Ref. [39]. Similarly, the errors seen in the 150% ETR case at low frequencies for small inlet angles are not yet accounted for.

B. Four Characteristics of BBSAN

In nonideally expanded, laboratory-scale jet noise, as well as in theoretical models, the BBSAN spectral shape has several distinctive

characteristics. The distinctive BBSAN spectral shape is steeper on the low-frequency side of the peak than on the high-frequency side. Possible spectral models for this shape are described in Sec II.B. The distinctive BBSAN spectral shape is seen in both the F-35B BBSAN (see Fig. 2a) and F/A-18E BBSAN (in Fig. 13 of Ref. [18]).

Some questions exist as to whether trends in other characteristics observed in laboratory-scale studies agree with BBSAN from high-performance military aircraft. Vaughn et al. [32] show the spatial variation in F-35B BBSAN peak level, frequency, and bandwidth of the top 3 dB of the spectra across the ground-based array at 75, 100, 130, and 150% ETR. In the current analysis, the BBSAN model parameters, L_{peak} , f_{peak} , and w_{sh} in Eq. (2), for the afterburning conditions (130 and 150% ETR) are compared to those reported for a tied-down F/A-18E reported by Tam et al. in Ref. [18]. While some of these BBSAN characteristics are the same as for laboratory-scale BBSAN, others are quite different. As the F-35B and F/A-18E BBSAN modeling efforts currently lead to different conclusions, a direct comparison is provided between the two sets of results.

The first BBSAN property of interest is the peak frequency. In nonideally expanded, laboratory-scale jets, the BBSAN peak frequency increases as the inlet angle increases. Early researchers related this increase in peak frequency to constructive interference [4] and perhaps a Doppler effect, at least qualitatively [22]. This shift in peak frequency has also been explained by Tam's wavy wall analogy [23,31]. Liu et al. [55] report that in large-eddy simulations of underexpanded jet flow, the increase in BBSAN peak frequency in the near field corresponds with a decrease in the shock-cell size. In agreement with laboratory-scale observations, the measured F-35B BBSAN at 75, 100, 130, and 150% ETR all show this same increase in peak frequency with an inlet angle [32]. For comparison, the afterburning F-35B BBSAN f_{peak} are displayed in Fig. 7a along with those reported in Table 2 of Ref. [18] for the afterburning F/A-18E BBSAN. For both aircraft, the variation agrees with the laboratory-scale trend.

The second BBSAN characteristic is the peak spectral level L_{peak} . In laboratory-scale measurements of BBSAN, L_{peak} decreases as the inlet angle increases. Vaughn et al. [32] showed that peak PSD values for the F-35B BBSAN follow this same trend for F-35B BBSAN at 75% ETR, but not for higher ETR. For the F-35B engine at afterburner, L_{peak} after scaling to a common distance first increases slightly then decreases; the change in L_{peak} with inlet angle, relative to L_{max} , the maximum level at each afterburning condition, is shown in Fig. 7b. The total variation in L_{peak} across the angular aperture is less than 4 dB, but as peak PSD levels from repeated measurements deviated by approximately 1 dB [32], the 4 dB change can be considered a physical feature of the afterburning F-35B BBSAN. In contrast, the afterburning F/A-18E L_{peak} (from Table 2 of Ref. [18]) increases by less than 2 dB as the inlet angle increases over an angular range of 35–65 deg. No indication is given as the uncertainty associated with the F/A-18E levels, and it is puzzling that the authors used only four measurement locations to identify a contrary trend of increasing L_{peak} since seven points are used to confirm the trend of increasing peak frequency. Only the last of the F/A-18E points does not follow the trends of the F-35B L_{peak} .

The conclusion for the afterburning F-35B BBSAN is that L_{peak} increases slightly (from 35 to approximately 50 deg) and agrees with the far-field spectral levels of the F-35B on a 76 m arc [49] and those shown for an uninstalled "current supersonic exhaust engine at high set point" in Fig. 6 of Ref. [14]. For this uninstalled engine, the peaks level of the BBSAN increases approximately 3 dB between 35 and 50 deg, similar to the increase seen in Fig. 7b. The combined peak spectral level for the uninstalled engine noise is relatively flat for inlet angles larger than 50 deg, in agreement with the measured peak levels of the F-35B BBSAN at 130 and 150% ETR shown in Fig. 4b of Ref. [32]. While the peak level of the measured PSD remains relatively constant for inlet angles larger than 50 deg, the L_{peak} values used to model the BBSAN spectra in Eq. (2), which are shown in Fig. 7b, decrease as inlet angle increases above 50 deg as the level of turbulent mixing noise increases dramatically. This comparison between the uninstalled and installed engine noise at high engine power shows that the increase and then decrease of the BBSAN level

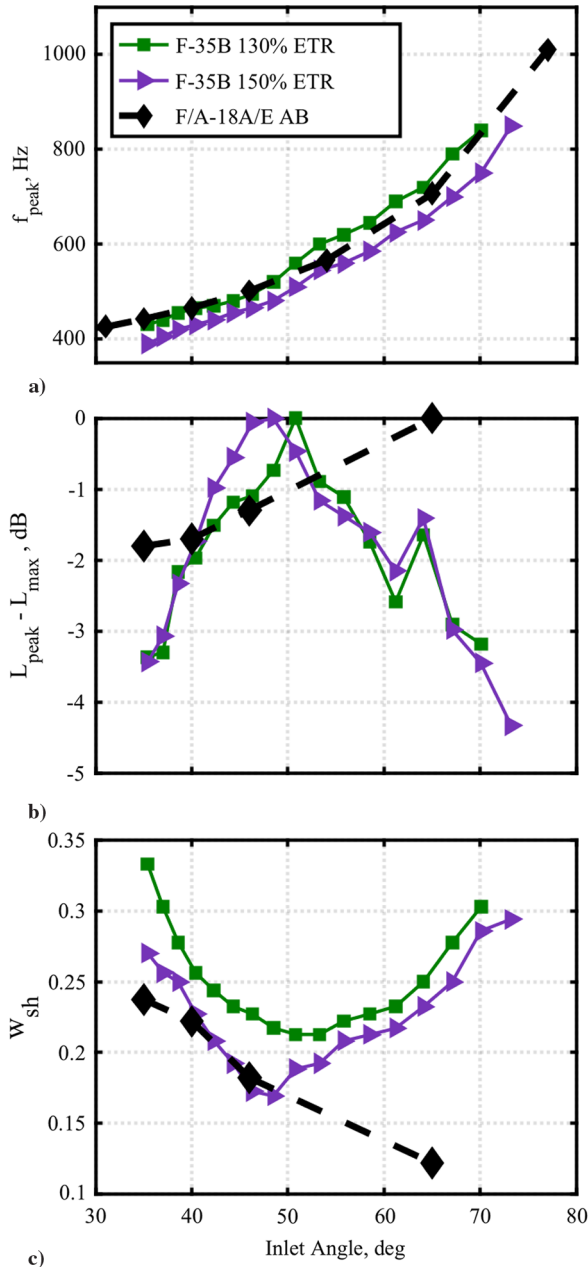


Fig. 7 BBSAN model parameters for F-35B at 130% ETR (green squares) and 150% ETR (purple triangles) and afterburning F/A-18E (black diamonds) (from Ref. [18]): a) f_{peak} , b) $L_{\text{peak}} - L_{\text{max}}$, and c) w_{sh} .

with inlet angle is not an installation effect and signals a difference from laboratory-scale BBSAN.

The third BBSAN characteristic is the width of the BBSAN spectral model [w_{sh} in Eq. (2)]. In nonideally expanded, laboratory-scale jets, this width increases as the inlet angle increases. The afterburning F/A-18E BBSAN was reported to have the opposite behavior: the width decreases as the inlet angle increases. The F/A-18E widths (from Table 2 of Ref. [18]) are compared to the afterburning F-35B in Fig. 7c. For the F-35B, w_{sh} increases as the inlet angle increases from 35 to approximately 50 deg and then decreases at larger inlet angles. Remarkable agreement is seen between w_{sh} of the F-35B at 150% ETR and the first three F-18E measurement locations, but w_{sh} reported for the fourth location differs greatly. The reason for this difference is unknown. The trend of decreasing then increasing w_{sh} , shown here for the F-35B afterburning cases, is also observed on the linear ground array near the F-35B aircraft at 75 and 100% ETR [32] and on a 76 m arc at all four ETR. The decrease in width of the F-35B BBSAN over an approximate angular aperture of 35–50 deg occurs at the same angles

Table 1 Comparison of BBSAN features for laboratory-scale jets and afterburning F-35B (in this paper) and F/A-18E (reported in Ref. [18]) [trends with increasing inlet angle are reported for f_{peak} , L_{peak} , and w_{sh} in Eq. (2)]

Parameter	Laboratory-scale BBSAN	F-35B BBSAN	F/A-18E BBSAN
f_{peak}	Increases	Increases	Increases
L_{peak}	Decreases	Increases then decreases	Increases
w_{sh}	Increases	Decreases then increases	Decreases

at which L_{peak} increases and is opposite the expected laboratory-scale trend. Additional investigation is required to determine the cause.

To summarize the similarities and differences between laboratory jet and high-performance military aircraft jet noise, the trends for each characteristic are compiled in Table 1. In all cases, the BBSAN is observed in the forward and sideline directions and has the same distinctive spectral shape and increase in peak frequency as the inlet angle increases. While the trends in peak level and width used in the BBSAN spectral model for the F/A-18E in Ref. [18] are reportedly the opposite of those seen in laboratory-scale studies, the F-35 BBSAN has the same trends as laboratory scale for angles greater than approximately 50 deg relative to the MARP (corresponding to less than 101 deg relative to the nozzle exit plane). The cause of the differences for smaller inlet angles is unknown but is likely related to the engine power since the F-35 BBSAN at 75% ETR shows a decrease in peak level at angles less than 50 deg but the same trend in width [32].

VI. Conclusions

A spectral decomposition has been applied to measurements near a tied-down F-35B that provides insight into the spatial variation in turbulent mixing noise and broadband shock-associated noise from a high-performance military aircraft engine. Many of the observations from measurements near a different full-scale jet aircraft [15] about turbulent mixing noise similarity spectra models have been confirmed, and the applicability of the Kuo et al. [31] broadband shock-associated noise (BBSAN) spectral model for the F-35B BBSAN has been shown. Strengths and limitations of these models in describing noise from high-performance military aircraft engines have been described.

The spatial accuracy of the three-way spectral decomposition for the F-35B has been quantified with broadband error maps (from 20 Hz to 20 kHz) that indicate the quality of the modeled spectra and highlight remaining discrepancies. Over a small angular range, the similarity spectrum associated with fine-scale turbulent mixing noise matches the F-35B spectral density. Slightly farther downstream, a combination of the large- and fine-scale similarity spectra matches the F-35B spectral density, and the large-scale similarity spectrum alone matches just outside the maximum radiation region. In the maximum radiation region, however, the large-scale similarity spectrum captures only the overall shape of the F-35B spectral density and does not account for the multiple spectral peaks seen in the maximum radiation region [46–48]. In addition, the high-frequency slope of the F-35B spectral density is shallower than the large-scale similarity spectrum because of nonlinear propagation [50,51], and the low-frequency slope of the F-35B spectral density is steeper. The cause of the latter is not yet known, although it was also seen in previous aircraft engine noise measurements [15,16,38]. Aft of the maximum radiation region, the large-scale similarity spectrum matches the peak and high-frequency portions of the spectrum. For higher engine powers and the farthest downstream locations, the main radiation region shifts forward, and the peak frequency is sufficiently low such that a second combination region appears. A shift in spectral slope at high frequencies is matched by including the fine-scale similarity spectrum with the same peak frequency as that observed at smaller inlet angles, something also observed in large-eddy simulations of highly heated jet noise [13]. The similarity of these conclusions for the F-35B to the prior spectral decomposition [15] is significant because of the differences between the engines.

This detailed view of the F-35B turbulent mixing noise is also the first narrowband application of the similarity spectra to high-performance military aircraft noise.

The other unique part of this study has been the decomposition of the F-35B sound field at small inlet angles into the fine-scale similarity spectrum and a BBSAN spectral model. BBSAN was not analyzed in the prior study [15] because BBSAN was not evident in the one-third octave band spectra, although ringing in the autocorrelation function at low inlet angles indicated its presence [19,20]. In the narrowband F-35B spectral density, the characteristic BBSAN spectral peak exceeds the fine-scale turbulent mixing noise at inlet angles of 35–70 deg. Kuo et al.'s [31] model for the BBSAN spectrum matches the main BBSAN peak. The peak frequency of the BBSAN increases with the increasing inlet angle, as was seen in prior laboratory-scale studies and the initial investigation of F/A-18E BBSAN [18]. The angular variation in the peak level and width of the BBSAN at high engine powers differs from trends seen in laboratory-scale BBSAN. Laboratory-scale BBSAN decreases in peak level and increases in width with the increasing inlet angle. While a decrease in BBSAN peak level is seen at 75% engine thrust request (ETR) [32], the peak level of the afterburning F/A-35B BBSAN increases and then remains relatively constant as the inlet angle increases, a trend that was also shown for far-field, uninstalled engine noise at a high set point [14]. The width of the F-35B BBSAN at all ETRs decreases and then increases with the inlet angle. The difference between afterburning F-35B BBSAN and those reported for an afterburning F/A-18E [18] and laboratory-scale studies are summarized in Table 1. Another contradiction between the established BBSAN models is that the angular dependence on peak frequency yields estimates of convective speed that are much larger than those derived from the wavy-wall analogy based on far-field directivity, as discussed in Appendix A. This discrepancy was also observed for F/A-18E BBSAN [18]. Additional work is needed to clarify the relationship between the peak frequencies and estimates of the convective velocity and shock-cell length [56,57] as well as to explore spectral models for higher-frequency BBSAN components [52].

This three-way spectral decomposition helps identify where further investigation is needed to better understand noise sources from a high-performance military aircraft. In addition, these decompositions lay the groundwork for the development of a broadband equivalent source model for F-35B noise.

Appendix: Details of the Spectral Decomposition

Additional information and analyses about the F-35B spectral decomposition are provided herein. The angles used in these analyses, defined relative to the MARP, are compared to angles measured relative to the nozzle exit plane, which are typically used in laboratory-scale, far-field studies. The definition of angles is tied to how the similarity spectra may be applied in the geometric near-field (and acoustic midfield) regime of the F-35B measurements, as explained in the Introduction. Following this discussion, three analyses are presented. First, the spatial variations in the peak levels and frequencies associated with the LSS, FSS, and BBSAN models are compared for 75 and 150% ETR, in Appendix A.2. In Appendix A.3, the peak frequencies of the portion of the spectra assigned to BBSAN are used in conjunction with Eq. (1) in the main text to estimate convective speed and average shock-cell length. Similar to the results in Ref. [18] for BBSAN of an afterburning F/A-18E, Eq. (1) does not yield physically realistic values for the convective velocity, indicating additional studies are needed to understand the BBSAN from high-performance military aircraft engines. The final analysis included in Appendix A.4 is a preliminary attempt to fit the second partial of BBSAN as a second harmonic with the Kuo et al. [31] model for the BBSAN spectrum.

A.1. Considerations for the Geometric Near Field

Because the spectral models were developed using far-field, laboratory-scale jets, questions arise as to their applicability for noise measured closer to the jet. The study of a Mach 1.8, unheated jet [12]

provides insight into how the similarity spectra can be applied over a range of distances. Good agreement is shown between the similarity spectra and the spectral content of noise measured on a far-field arc and a set of close line arrays. The closer line arrays were at sideline distances of $x = 5$ and 10 nozzle diameters D from and parallel to the jet centerline. The similarity spectra did not account for the low-frequency hydrodynamic near-field noise at farther downstream distances on the $5D$ line array but captured the remaining spectral shapes. Examples of the similarity spectra decompositions at both the $10D$ line array and the far-field arc are shown in Figs. 5 and 6 of Ref. [12], and the large-scale and fine-scale similarity spectra and their combination are obtained. The far-field arc had a radius of $40D$ and was centered not around the nozzle exit but around a MARP located downstream at $z = 10D$. This choice is critical for the correct connection between the spectral decompositions of the different arrays. Specifically, the consistency provided in using the MARP to define angles is explored in Fig. 8 of Ref. [12]. When $z = 10D$ is used to define angles, the angular regions over which the FSS, LSS, and a combination of the two spectra apply agree between the $5D$ and $10D$ line arrays and the $40D$ arc. However, when $z = 5D$ or $z = 15D$ is used as an origin to define the angles, the type of spectral decomposition changes between the line arrays and the far-field arc. Thus, the selection of the MARP for defining angles is critical for correct application of the similarity spectra in the geometric near field (acoustic midfield). The nuances of how to define angles become less important as the distances become larger, which is why the prior far-field laboratory studies have not noticed these effects.

The Mach 1.8 laboratory-scale study in Ref. [12] provides confirmation of two things that are central to the F-35B spectral decompositions. First, the similarity spectra do describe laboratory-scale jet noise in the geometric near field (acoustic midfield). Second, when spectral models developed using far-field measurements are employed in the geometric near field, care must be taken when defining the angles.

This second point can be illustrated by considering how different definitions of angles would affect the interpretation of the F-35B spectral decompositions. On the measurement schematic in Fig. A1, 30 deg intervals for angles defined relative to the MARP are shown as blue lines, while 30 deg intervals relative to the nozzle exit plane are displayed as black lines. The type of spectral decomposition used to match the spectra at each microphone location for the 75% ETR case is indicated with the color: red for the LSS spectrum only, purple for a combination of LSS and FSS spectra, gray for the FSS spectrum only, and green for a combination of FSS and BBSAN spectra. Using the angles relative to the MARP, the LSS + FSS combination region lies between 80 and 107 deg. This angular aperture corresponds to angles relative to the nozzle exit plane of 127–140 deg, which all laboratory-scale literature would agree are much larger than the angles at which the combination of FSS and LSS spectra is expected. Thus, while the MARP might not be the exact location from which to define angles for spectral decompositions, angles relative to the MARP provide much better agreement with far-field angles than those defined relative to the nozzle exit plane.

A.2. Characteristics of Spectral Decomposition

The three-way spectral decomposition was performed at all 71 locations of the ground-based linear array near a tied-down F-35B. While there is latitude in fitting the spectral models to the PSD, the fits were guided by the goal of creating the best fit in the peak-frequency portion of each spectrum while maintaining smoothly varying OASPL and peak frequency, as described in Sec. IV. The contributions of each spectral component to the OASPL along with the measured OASPL as a function of inlet angle are displayed in Fig. A2. An outward spherical spreading correction is applied to scale the OASPL to a common distance of 30 m from the MARP; the spherical spreading assumption is reasonable in this case because the OASPL is dominated by frequencies not affected by the nonlinear propagation. At 75% ETR, the contribution to the OASPL from the FSS and LSS spectra increases and decreases as the inlet angle

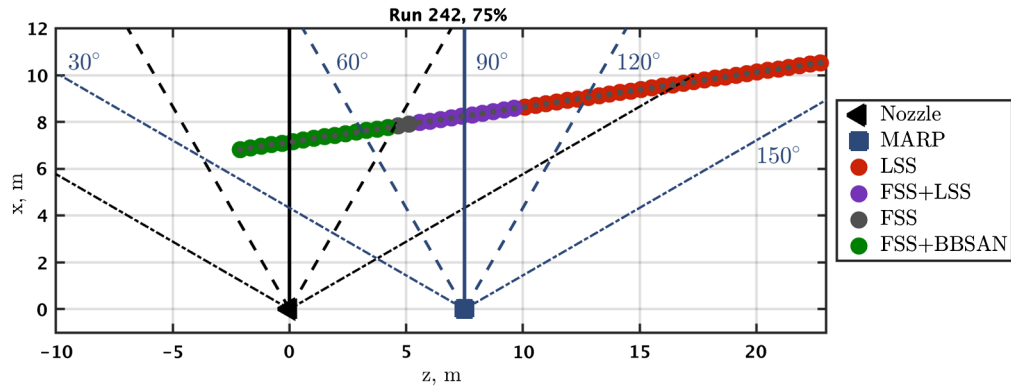


Fig. A1 Angles relative to the MARP (blue), angles relative to the nozzle exit plane (black), and the type of similarity spectra for 75% ETR at microphone locations.

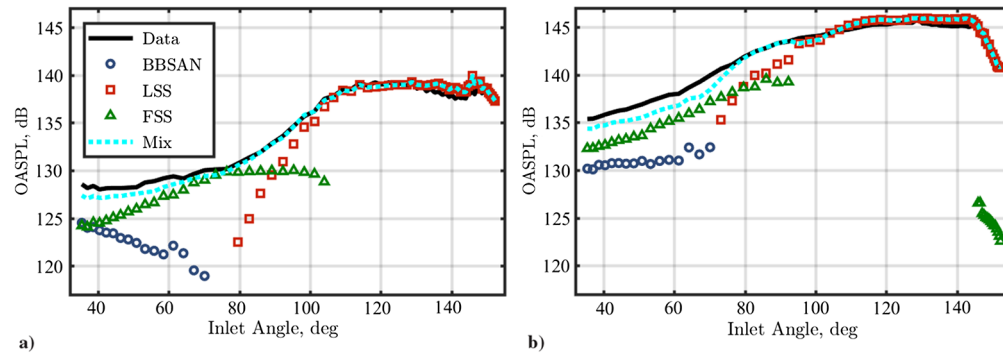


Fig. A2 F-35B OASPL (black) at a) 75% ETR and b) 150% ETR with the modeled spectral components: LSS (red), FSS (green), BBSAN (blue), and combination (cyan).

increases with the maximum contribution of the FSS spectrum occurring at inlet angles of 75–100 deg (relative to the MARP). At 150% ETR, similar trends are seen in the FSS and LSS levels. In both cases, the OASPL of the LSS component agrees with the measured OASPL in the relatively large maximum radiation region but does so by splitting the difference between the multiple spectral peaks, as illustrated in Fig. 4a. The relative contribution of BBSAN to the combined OASPL decreases as the inlet angle increases, and the turbulent mixing noise becomes more prominent. However, a difference is observed between 75 and 150% ETR. The decrease in level with the inlet angle, as at 75% ETR, agrees with prior laboratory-scale studies, while the slight increase seen at 150% ETR does not. This difference is examined in Ref. [32] and was discussed further in Sec. V.A.

The peak frequencies associated with the three spectral models also change as a function of angle. As shown in Fig. A3, the trends differ for each spectral model. The peak frequency of the BBSAN model increases with the inlet angle: from 570 Hz at 35 deg to approximately 1250 Hz at 70 deg for 75% ETR (Fig. A3a) and from

390 Hz at 35 deg to approximately 850 Hz at 70 deg for 150% ETR (Fig. A3b). In contrast, the peak frequency of the FSS spectrum remains constant across the entire angular range, both at smaller inlet angles and when it reemerges aft of the maximum radiation region. For 75% ETR, the LSS spectrum's peak frequency begins at 320 Hz around 80 deg and remains approximately constant over the combination region (80–105 deg). In the maximum radiation region, the peak frequency of the LSS spectrum decreases and then levels off around 100 Hz for $\theta > 140$ deg. At 150% ETR, a continually decreasing peak frequency is used for the LSS spectrum from 800 Hz at 70 deg to 50 Hz at 152 deg. These trends resemble the peak-frequency analysis of a different high-performance military aircraft engine shown in Ref. [15] as well as the variation in peak frequency shown for the high-temperature, laboratory-scale jet noise studies by Seiner et al. (see Fig. 16 of Ref. [42]). Closest to the jet axis for 150% ETR, after the strength of the large-scale turbulent mixing noise has diminished and its peak frequency has shifted low enough, the PSD is better matched by adding the FSS spectrum at a similar peak frequency as in Fig. 7.

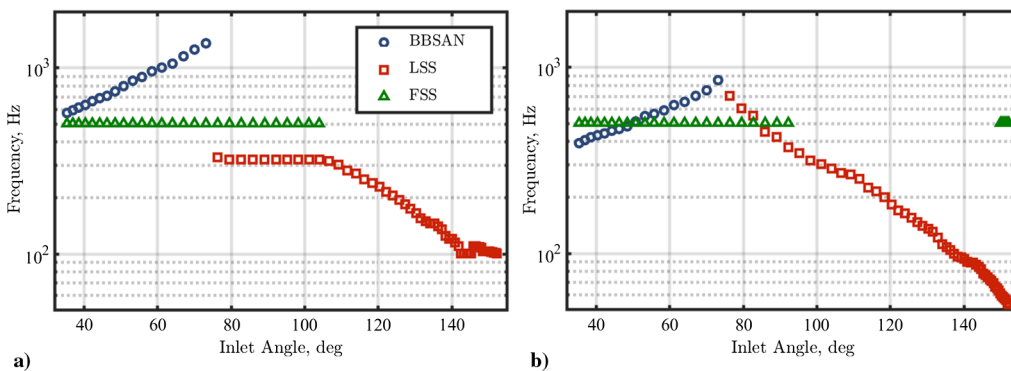


Fig. A3 Spatial variation in peak frequency of BBSAN (blue), FSS (green), and LSS (red) spectra.

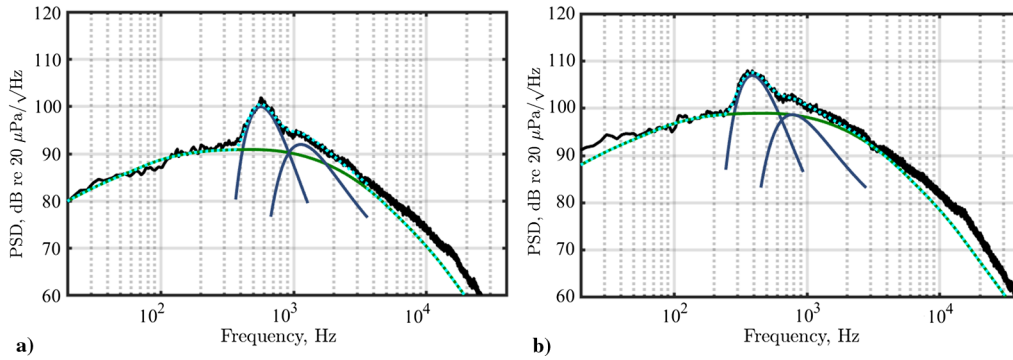


Fig. A4 F-35B PSD at a) 75% ETR (black) and b) 150% ETR decomposed into FSS spectrum (green) and BBSAN first and second harmonics (blue) with the total modeled PSD (cyan) at an inlet angle of 35.4 deg.

A.3. Estimates of Convective Velocity

In addition to the difference in the spatial variation of L_{peak} and w_{sh} between the F-35 BBSAN and laboratory-scale BBSAN studies, it appears that the application of Eq. (1) to afterburning military aircraft noise, or at least the interpretation thereof, is not straightforward. In this subsection, frequency-dependent convective velocity estimates obtained from Eq. (1) are compared to estimates based on far-field directivity. When placed in Eq. (1), the collection of measured f_{peak} as a function of θ (shown in Fig. A3a) yields a system of equations that can be solved via a least-squares method for u_c and L . For the F-35B at 150% ETR, the resulting estimated values are $u_c = 1620$ m/s and $L = 0.8$ m, similar to the values of $u_c = 1435$ m/s and $L = 0.7$ m for the F/A-18E afterburning case in Ref. [18]. While the values of L seem reasonable, the estimates of u_c are much larger than expected from the far-field directivity. A measurement arc located at 76 m (250 ft) from the MARP for the F-35B case has peak directivity angles between 125 and 140 deg, corresponding to convective speeds of 450–600 m/s, significantly lower than those estimated via the least-squares solution based on the BBSAN peak frequencies and Eq. (1).

A few possible reasons for this discrepancy exist. As postulated in Ref. [18], the BBSAN for an afterburning high-performance military aircraft engine could be a new noise mechanism, perhaps related to indirect combustion noise. A different interpretation is that the high-performance military engine noise reaches conditions (rarely seen in laboratory-scale measurements) in which three types of Mach waves are present. The corresponding Mach numbers for these three types of Mach waves were given by Oertel [56], and a theoretical basis for them was presented in Tam and Hu [57]. Seiner et al. [42] showed that, while the Kelvin–Helmholtz instability waves dominate the noise generation at lower jet temperatures, at higher temperatures, a second type of Mach wave, referred to as the supersonic instability wave, appears. The third type of Mach wave was subsonic in all prior laboratory-scale studies. Possibly the different types of Mach waves are present in the high-performance military aircraft engine noise and interact with the shock cells in a manner that complicates the applicability of Eq. (1). Another possibility could be related to the effect observed by Liu et al. [45] in which comparisons between large-eddy simulations of ideally and underexpanded jets showed that the angular variation in the peak frequency in the near field relates to changes in shock-cell size. Further investigation is needed to determine how the variation in f_{peak} as a function of θ is related to the convective velocities for high-performance military aircraft noise.

A.4. Higher-Frequency BBSAN

The final analysis is a preliminary investigation into higher-frequency components of BBSAN that can be seen in the F-35B PSD at the smallest inlet angles. In the Harper-Bourne and Fisher [4] model, higher harmonics of BBSAN were proposed but not evident in their data. In the original Tam [28–30] model for the BBSAN spectrum, the higher-frequency BBSAN corresponds to higher-order modal frequencies of the waveguide created by the quasi-periodic shock-cell structure, as described in Sec. II.B, that are not

harmonically related. Unfortunately, the Tam BBSAN model requires knowledge of jet parameters that were unavailable for the F-35B. Instead, as a preliminary attempt at fitting the second BBSAN component, Kuo et al.'s [31] BBSAN model is employed but for a second harmonic that is wider by a factor of $\sqrt{2}$; the parameters $f_{\text{peak},2} = 2f_{\text{peak}}$ and $w_{\text{sh},2} = \sqrt{2}w_{\text{sh}}$ are used in Fig. A4 to generate a second BBSAN spectral peak for the 35.4 deg at 75% ETR (part a) and 150% ETR (part b). The second harmonic significantly increases the agreement between the measured and modeled spectral levels over the 1000–3000 Hz band. The marked improvement in the fit using a second harmonic with a width scaled by $\sqrt{2}$ is significant because those match the characteristics of harmonic generation through a quadratic nonlinear process [52]. While uncertainty remains as whether the cause is related to a nonlinear mode coupling in the BBSAN noise source or some other mechanism, this preliminary investigation shows that further work should be done in developing a model for the higher-frequency components of BBSAN for high-performance military aircraft noise.

Acknowledgments

The authors gratefully acknowledge funding for the measurements, provided through the F-35B Program Office and U.S. Air Force Research Laboratory. The authors thank the reviewers for their feedback in clarifying key points in this Paper. Analysis was supported in part through a grant from the U.S. Office of Naval Research, grant number N000141410494. This work has been cleared for Distribution A: Approved for public release; distribution is unlimited. F-35 PAO cleared 09/10/2018; JSF18-916).

References

- [1] Tam, C. K. W., "Supersonic Jet Noise," *Annual Review of Fluid Mechanics*, Vol. 27, No. 1, 1995, pp. 17–43. doi:10.1146/annurev.fl.27.010195.000313
- [2] Tam, C. K. W., "Jet Noise: Since 1952," *Theoretical and Computational Fluid Dynamics*, Vol. 10, Nos. 1–4, 1998, pp. 393–405. doi:10.1007/s001620050072
- [3] Viswanathan, K., "Aeroacoustics of Hot Jets," *Journal of Fluid Mechanics*, Vol. 516, Oct. 2004, pp. 39–82. doi:10.1017/S0022112004000151
- [4] Harper-Bourne, M., and Fisher, M. J., "The Noise from Shockwaves in Supersonic Jets," AGARD, CP-131, 1974, pp. 11.1–11.13.
- [5] Petitjean, B. P., Viswanathan, K., and McLaughlin, D. K., "Acoustic Pressure Waveforms Measured in High Speed Jet Noise Experiencing Nonlinear Propagation," *International Journal of Aeroacoustics*, Vol. 5, No. 2, 2006, pp. 193–215. doi:10.1260/14754720677629835
- [6] Schlinker, R. H., "Supersonic Jet Noise Experiments," Ph.D. Dissertation, Univ. of Southern California, Los Angeles, CA, 1975.
- [7] Laufer, J., Schlinker, R., and Kaplan, R. E., "Experiments on Supersonic Jet Noise," *AIAA Journal*, Vol. 14, No. 4, 1976, pp. 489–497. doi:10.2514/3.61388
- [8] Tam, C. K. W., Viswanathan, K., Ahuja, K. K., and Panda, J., "The Sources of Jet Noise: Experimental Evidence," *Journal of Fluid Mechanics*, Vol. 615, Nov. 2008, pp. 253–292. doi:10.1017/S0022112008003704

- [9] Viswanathan, K., "Analysis of the Two Similarity Components of Turbulent Mixing Noise," *AIAA Journal*, Vol. 40, No. 9, 2002, pp. 1735–1744.
doi:10.2514/2.1878
- [10] Tam, C. K. W., Golebiowsky, M., and Seiner, J. M., "On the Two Components of Turbulent Mixing Noise from Supersonic Jets," AIAA Paper 1996-1716, May 1996.
doi:10.2514/6.1996-1716
- [11] Tam, C. K. W., and Zaman, K., "Subsonic Noise from Nonaxisymmetric and Tabbed Nozzles," *AIAA Journal*, Vol. 38, No. 4, 2000, pp. 592–599.
doi:10.2514/3.14449
- [12] Vaughn, A. B., Neilsen, T. B., Gee, K. L., Okamoto, K., and Akamine, M., "Near-Field Spatial Variation in Similarity Spectra Decomposition of a Mach 1.8 Laboratory-Scale Jet," *Proceedings of Meetings on Acoustics*, Vol. 29, Paper 045004, 2016, pp. 0–10.
doi:10.1121/2.0000456
- [13] Liu, J., Kailasanath, K., and Gutmark, E. J., "Similarity Spectra of Highly Heated Supersonic Jets Using Large-Eddy Simulations," AIAA Paper 2017-0926, 2017.
doi:10.2514/6.2017-0926
- [14] Schlinker, R. H., Liljenberg, S. A., Polak, D. R., Post, K. A., Chipman, C. T., and Stern, A. M., "Supersonic Jet Noise Source Characteristics & Propagation: Engine and Model Scale," AIAA Paper 2007-3623, 2007.
doi:10.2514/6.2007-3623
- [15] Neilsen, T. B., Gee, K. L., Wall, A. T., and James, M. M., "Similarity Spectra Analysis of High-Performance Jet Aircraft Noise," *Journal of the Acoustical Society of America*, Vol. 133, No. 4, 2013, pp. 2116–2125.
doi:10.1121/1.4792360
- [16] McKinley, R., McKinley, R., Gee, K. L., Pilon, T., Mobley, F., Gillespie, M., and Downing, J. M., "Measurement of Near-Field and Far-Field Noise from Full-Scale High-Performance Jet Engines," *Proceedings of ASME Turbo Expo 2010*, American Soc. of Mechanical Engineers Paper GT2010-22531, Glasgow, Scotland, June 2010.
- [17] Neilsen, T. B., Gee, K. L., Wall, A. T., James, M. M., and Atchley, A. A., "Comparison of Supersonic Full-Scale and Laboratory-Scale Jet Data and the Similarity Spectra for Turbulent Mixing Noise," *Proceedings of Meetings on Acoustics*, Vol. 19, Paper 040071, 2013, pp. 0–8.
doi:10.1121/1.4799664
- [18] Tam, C. K. W., Aubert, A. C., Spyropoulos, J. T., and Powers, R. W., "On the Dominant Noise Components of Tactical Aircraft: Laboratory to Full Scale," *Journal of Sound and Vibration*, Vol. 422, May 2018, pp. 92–111.
doi:10.1016/j.jsv.2018.02.023
- [19] Harker, B. M., Neilsen, T. B., Gee, K. L., Wall, A. T., McNerny, S. A., and James, M. M., "On Autocorrelation Analysis of Jet Noise," *Journal of the Acoustical Society of America*, Vol. 133, No. 6, 2013, pp. EL458–EL464.
doi:10.1121/1.4802913
- [20] Harker, B. M., Neilsen, T. B., Gee, K. L., Wall, A. T., and James, M. M., "Spatiotemporal Correlation Analysis of Jet Noise from a High-Performance Military Aircraft," *AIAA Journal*, Vol. 54, No. 5, 2016, pp. 1554–1566.
doi:10.2514/1.J054442
- [21] Faranosov, G. A., Belyaev, I. V., Kopiev, V. F., Zaytsev, M. Y., Aleksentsev, A. A., Bersenev, Y. V., Chursin, V. A., and Viskova, T. A., "Adaptation of the Azimuthal Decomposition Technique to Jet Noise Measurements in Full-Scale Tests," *AIAA Journal*, Vol. 55, No. 2, 2017, pp. 572–584.
doi:10.2514/1.J055001
- [22] Seiner, J. M., and Norum, T. D., "Experiments of Shock Associated Noise of Supersonic Jets," AIAA Paper 1979-1526, 1979.
- [23] Norum, T. D., and Seiner, J. M., "Broadband Shock Noise from Supersonic Jets," *AIAA Journal*, Vol. 20, No. 1, 1982, pp. 68–73.
doi:10.2514/3.51048
- [24] Seiner, J. M., and Yu, J. C., "Acoustic Near-Field Properties Associated with Broadband Shock Noise," *AIAA Journal*, Vol. 22, No. 9, 1984, pp. 1207–1215.
doi:10.2514/3.8762
- [25] Tanna, H. K., "An Experimental Study of Jet Noise Part II: Shock Associated Noise," *Journal of Sound and Vibration*, Vol. 50, No. 3, 1977, pp. 429–444.
doi:10.1016/0022-460X(77)90494-1
- [26] Pao, S. P., and Seiner, J. M., "Shock-Associated Noise in Supersonic Jets," *AIAA Journal*, Vol. 21, No. 5, 1983, pp. 687–693.
doi:10.2514/3.8134
- [27] Panda, J., and Seasholtz, R. G., "Measurements of Shock Structure and Shock-Vortex Interaction in Underexpanded Jets Using Rayleigh Scattering," *Physics of Fluids A: Fluid Dynamics*, Vol. 11, No. 12, 1999, pp. 3761–3777.
doi:10.1063/1.870247
- [28] Tam, C. K. W., and Tanna, H. K., "Shock Associated Noise of Supersonic Jets from Convergent-Divergent Nozzles," *Journal of Sound and Vibration*, Vol. 81, No. 3, 1982, pp. 337–358.
doi:10.1016/0022-460X(82)90244-9
- [29] Tam, C. K. W., "Stochastic Model Theory of Broadband Shock Associated Noise from Supersonic Jets," *Journal of Sound and Vibration*, Vol. 116, No. 2, 1987, pp. 265–302.
doi:10.1016/S0022-460X(87)81303-2
- [30] Tam, C. K. W., "Broadband Shock Associated Noise of Moderately Imperfectly Expanded Supersonic Jets," *Journal of Sound and Vibration*, Vol. 140, No. 1, 1990, pp. 55–71.
doi:10.1016/0022-460X(90)90906-G
- [31] Kuo, C. W., McLaughlin, D. K., Morris, P. J., and Viswanathan, K., "Effects of Jet Temperature on Broadband Shock-Associated Noise," *AIAA Journal*, Vol. 53, No. 6, 2015, pp. 1515–1530.
doi:10.2514/1.J053442
- [32] Vaughn, A. B., Neilsen, T. B., Gee, K. L., Wall, A. T., Downing, J. M., and James, M. M., "Broadband Shock-Associated Noise of a High-Performance Military Aircraft," *Journal of the Acoustical Society of America*, Vol. 144, No. 3, 2018, pp. EL242–EL247.
doi:10.1121/1.5055392
- [33] Viswanathan, K., Alkislal, M. B., and Czech, M. J., "Characteristics of the Shock Noise Component of Jet Noise," *AIAA Journal*, Vol. 48, No. 1, 2010, pp. 25–46.
doi:10.2514/1.38521
- [34] Viswanathan, K., "Scaling Laws and a Method for Identifying Components of Jet Noise," *AIAA Journal*, Vol. 44, No. 10, 2006, pp. 2274–2285.
doi:10.2514/1.18486
- [35] Neilsen, T. B., Gee, K. L., and James, M. M., "Spectral Characterization in the near and Mid-Field of Military Jet Aircraft Noise," AIAA Paper 2013-2191, June 2013.
doi:10.2514/6.2013-2191
- [36] Wall, A. T., Gee, K. L., James, M. M., Bradley, K. A., McNerny, S. A., and Neilsen, T. B., "Near-Field Noise Measurements of a High-Performance Military Jet Aircraft," *Noise Control Engineering Journal*, Vol. 60, No. 4, 2012, pp. 421–434.
doi:10.3397/1.3701021
- [37] Petitjean, B. P., and McLaughlin, D. K., "Experiments on the Nonlinear Propagation of Noise from Supersonic Jets," AIAA Paper 2003-3127, 2003.
doi:10.2514/6.2003-3127
- [38] Gee, K. L., Gabrielson, T. B., Atchley, A. A., and Sparrow, V. W., "Preliminary Analysis of Nonlinearity in Military Jet Aircraft Noise Propagation," *AIAA Journal*, Vol. 43, No. 6, 2005, pp. 1398–1401.
doi:10.2514/1.10155
- [39] Gee, K. L., Sparrow, V. W., James, M. M., Downing, J. M., Hobbs, C. M., Gabrielson, T. B., and Atchley, A. A., "The Role of Nonlinear Effects in the Propagation of Noise from High-Power Jet Aircraft," *Journal of the Acoustical Society of America*, Vol. 123, No. 6, 2008, pp. 4082–4093.
doi:10.1121/1.2903871
- [40] Gee, K. L., Neilsen, T. B., Downing, J. M., James, M. M., McKinley, R. L., McKinley, R. C., and Wall, A. T., "Near-Field Shock Formation in Noise Propagation from a High-Power Jet Aircraft," *Journal of the Acoustical Society of America*, Vol. 133, No. 2, 2013, pp. EL88–EL93.
doi:10.1121/1.4773225
- [41] Gee, K. L., Neilsen, T. B., Wall, A. T., Downing, J. M., James, M. M., and McKinley, R. L., "Propagation of Crackle-Containing Noise from Military Jet Aircraft," *Noise Control Engineering Journal*, Vol. 64, No. 1, 2016, pp. 0–12.
doi:10.3397/1/376354
- [42] Seiner, J. M., Ponton, M. K., Jansen, B. J., and Lagen, N. T., "The Effects of Temperature on Supersonic Jet Noise Emission," AIAA Paper 92-02-46, May 1992, pp. 295–307.
- [43] Oertel, H., "Measured Velocity Fluctuations Inside the Mixing Layer of a Supersonic Jet," *Recent Contributions to Fluid Mechanics*, edited by W. Haas, Springer-Verlag, Berlin, 1982, pp. 170–179.
doi:10.1007/978-3-642-81932-2_18
- [44] Tam, C. K. W., and Hu, F. Q., "On the Three Families of Instability Waves of High-Speed Jets," *Journal of Fluid Mechanics*, Vol. 201, April 1989, pp. 447–483.
doi:10.1017/S002211208900100X
- [45] Liu, J., Corrigan, A., Kailasanath, K., and Taylor, B., "Impact of the Specific Heat Ratio on Noise Generation of a High-Temperature

- Supersonic Jet,” AIAA Paper 2016-2125, Jan. 2016.
doi:10.2514/6.2016-2125
- [46] Wall, A. T., Leete, K. M., Gee, K. L., Neilsen, T. B., James, M. M., and McKinley, R. L., “Preliminary Investigation of Multilobe Fighter Jet Noise Sources Using Acoustical Holography,” AIAA Paper 2017-3520, June 2017.
doi:10.2514/6.2017-3520
- [47] Leete, K. M., Wall, A. T., Gee, K. L., Neilsen, T. B., James, M. M., and Downing, J. M., “Dependence of High-Performance Military Aircraft Noise on Frequency and Engine Power,” AIAA Paper 2018-2826, June 2018.
doi:10.2514/6.2018-2826
- [48] Swift, H. S., Gee, K. L., Neilsen, T. B., Wall, A. T., Downing, J. M., and James, M. M., “Spatiotemporal Correlation Analysis of Jet Noise from a Round-Nozzle Supersonic Aircraft,” AIAA Paper 2018-3938, 2018.
doi:10.2514/6.2018-3938
- [49] James, M. M., Salton, A. R., Downing, J. M., Gee, K. L., Neilsen, T. B., Reichman, B. O., McKinley, R. L., Wall, A. T., and Gallagher, H. L., “Acoustic Emissions from F-35B Aircraft During Ground Run-Up,” AIAA Paper 2015-2375, June 2015.
doi:10.2514/6.2015-2375
- [50] Reichman, B. O., Wall, A. T., Gee, K. L., Neilsen, T. B., Downing, J. M., James, M. M., and McKinley, R., “Modeling Far-Field Acoustical Nonlinearity from F-35B Aircraft During Ground Run-Up,” AIAA Paper 2016-1888, Jan. 2016.
doi:10.2514/6.2016-1888
- [51] Reichman, B. O., Gee, K. L., Neilsen, T. B., Swift, S. H., Wall, A. T., Gallagher, H. L., Downing, J. M., and James, M. M., “Acoustic Shock Formation in Noise Propagation During Ground Run-Up Operations of Military Aircraft,” AIAA Paper 2017-4043, June 2017.
- [52] Gurbatov, S. N., and Rudenko, O. V., “Statistical Phenomena,” *Nonlinear Acoustics*, edited by M. F. Hamilton, and D. T. Blackstock, Academic Press, New York, 1998, pp. 377–398, Chap. 13.
- [53] Reichman, B. O., Muhlestein, M. B., Gee, K. L., Neilsen, T. B., and Thomas, D. C., “Evolution of the Derivative Skewness for Nonlinearly Propagating Waves,” *Journal of the Acoustical Society of America*, Vol. 139, No. 3, 2016, pp. 1390–1403.
doi:10.1121/1.4944036
- [54] Stout, T. A., Gee, K. L., Neilsen, T. B., Wall, A. T., and James, M. M., “Source Characterization of Full-scale Jet Noise Using Acoustic Intensity,” *Noise Control Engineering Journal*, Vol. 63, No. 6, 2015, pp. 522–536.
doi:10.3397/1/376346
- [55] Liu, J., Corrigan, A. T., Kailasanath, K., Heeb, N. S., and Gutmark, E. J., “Numerical Study of Noise Sources Characteristics in an Under-expanded Jet Flow,” AIAA Paper 2014-2604, 2014.
- [56] Oertel, H., “Measured Velocity Fluctuations Inside the Mixing Layer of a Supersonic Jet,” *Recent Contributions to Fluid Mechanics*, edited by W. Haas, Springer-Verlag, Berlin, 1982, pp. 170–179.
doi:10.1007/978-3-642-81932-2_18
- [57] Tam, C. K. W., and Hu, F. Q., “On the Three Families of Instability Waves of High-Speed Jets,” *Journal of Fluid Mechanics*, Vol. 201, April 1989, pp. 447–483.
doi:10.1017/S002211208900100X

L. Ukeiley
Associate Editor